

# Computational Study of Turbulent-Laminar Patterns in Couette Flow

Dwight Barkley\*

Mathematics Institute, University of Warwick, Coventry CV4 7AL, United Kingdom

Laurette S. Tuckerman†

LIMSI-CNRS, BP 133, 91403 Orsay, France

(Dated: February 26, 2018)

Turbulent-laminar patterns near transition are simulated in plane Couette flow using an extension of the minimal flow unit methodology. Computational domains are of minimal size in two directions but large in the third. The long direction can be tilted at any prescribed angle to the streamwise direction. Three types of patterned states are found and studied: periodic, localized, and intermittent. These correspond closely to observations in large aspect ratio experiments.

Plane Couette flow – the flow between two infinite parallel plates moving in opposite directions – undergoes a subcritical (discontinuous) transition from laminar flow to turbulence as the Reynolds number is increased. Due to its simplicity, this flow has long served as one of the canonical examples for understanding shear turbulence and the subcritical transition process typical of channel and pipe flows [1, 2, 3, 4, 5, 6, 7, 8, 9, 10, 11, 12]. Only recently was it discovered in very large aspect ratio experiments by Prigent *et al.* [13, 14, 15] that this flow also exhibits remarkable pattern formation near transition. Figure 1 shows such a pattern, not from experiment, but from numerical computations reported here. An essentially steady, spatially periodic pattern of distinct regions of turbulent and laminar flow emerges spontaneously from uniform turbulence as the Reynolds number is decreased. It now appears that turbulent-laminar patterns are inevitable intermediate states on the route from turbulent to laminar flow in large aspect ratio plane Couette flow.

Related patterns have a long history in fluid dynamics. In Taylor-Couette flow between counter-rotating cylinders, Coles [16] first discovered a state known as spiral turbulence with coexisting turbulent and laminar regions. This state was famously commented on by Feynman [17] and has attracted attention as an example of a coherent structure comprising both turbulence and long-range order [18, 19, 20, 21]. Until recently all experimental studies of this state showed only one turbulent and one laminar patch. Prigent *et al.* [13, 14, 15] found that in a very large-aspect-ratio Taylor-Couette system, the turbulent and laminar regions form a periodic pattern, of which the original observations of Coles comprised only one wavelength. Cros and Le Gal [22] discovered large-scale turbulent spirals as well, in experiments on the shear flow between a stationary and a rotating disk. The Reynolds-number thresholds, wavelengths, and angles are very similar for all of these turbulent patterned flows. Moreover, Prigent *et al.* suggest that the turbulent spots [2, 3, 4, 6, 8, 10, 12, 22, 23] long known to exist near transition are essentially a manifestation of the same mechanism.

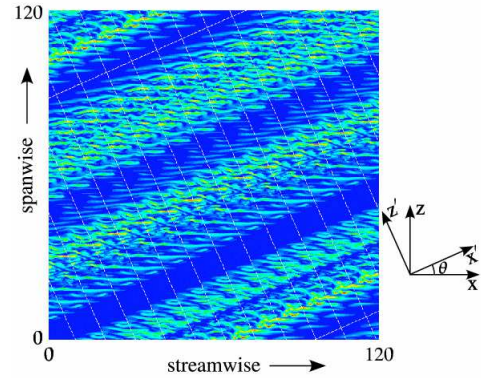


FIG. 1: Turbulent-laminar pattern at Reynolds number 350. The computational domain (outlined in white, aligned along  $x', z'$ ) is repeated periodically to tile an extended region. The kinetic energy is visualized in a plane midway between and parallel to the plates moving in the streamwise ( $x$ ) direction. Uniform gray or blue corresponds to laminar flow. The sides of the image are 60 times the plate separation  $L_y = 2$ ; the pattern wavelength is  $20 L_y$ . Streamwise streaks (on the scale of  $L_y$ ) are visible at the edges of the turbulent regions.

We report the first direct numerical simulation of turbulent-laminar patterns. Our simulations are designed to reduce computational expense, to establish minimal physical conditions necessary to produce these large-scale patterns, and to impose and thereby investigate the pattern wavelength and orientation.

Our study extends minimal-flow-unit (MFU) simulations of turbulent channel flows [1, 5, 9] and we begin by recalling these. The plates located at  $y = \pm 1$  move at unit velocities  $\pm \hat{\mathbf{x}}$ . The Reynolds number is  $Re = 1/\nu$ , where  $\nu$  is the kinematic viscosity of the fluid. The simple Couette solution  $\mathbf{u}_C \equiv y\hat{\mathbf{x}}$  is linearly stable for all values of  $Re$ . However, above a critical  $Re$  near 325 [6], transition to turbulence occurs for sufficiently large perturbations. The turbulence is characterized by the cyclical generation and breakdown of streaks by streamwise-oriented vortices with a natural spanwise pair spacing of about 4 [1, 5, 9, 23, 24]. In the MFU approach, a

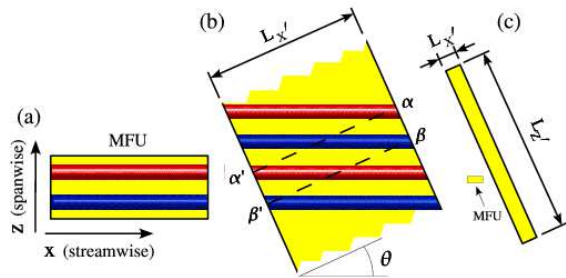


FIG. 2: Simulation domains. The wall-normal direction  $y$  is not seen;  $L_y = 2$ . The gray or colored bars represent streamwise vortex pairs with a spanwise spacing of 4. (The vortices are schematic; these are dynamic features of the actual flow.) (a) MFU domain of size  $10 \times 4$ . (b) Central portion of a domain [on the same scale as (a)] tilted to the streamwise direction.  $\alpha$ ,  $\alpha'$  and  $\beta$ ,  $\beta'$  are pairs of points identified under periodic boundary conditions in  $x'$ . (c) Full tilted domain with  $L_{x'} = 10$ ,  $L_{z'} = 120$ ,  $\theta = 24^\circ$ . On this scale the MFU domain, shown for comparison, is small.

periodic domain of minimal lateral dimensions is sought which can sustain this basic cycle. For plane Couette flow near transition, the currently accepted [9] size is approximately  $L_x \times L_z = 10 \times 4$  [Fig. 2(a)].

We extend the MFU computations in two ways. First we tilt the domain at angle  $\theta$  to the streamwise direction [Fig. 2(b)]. We designate by  $x'$  and  $z'$  the periodic directions of the tilted domain. To respect the spanwise streak spacing while imposing periodic boundary conditions in  $x'$ , the domain satisfies  $L_{x'} \sin \theta \simeq 4$ , for  $\theta > 0$ . (For  $\theta = 0$ , we only require  $L_{x'} \gtrsim 10$ .) Secondly, we greatly extend one of the dimensions past the MFU requirement [Fig. 2(c)]. In practice we use  $L_{z'}$  between 30 and 220, usually 120. We can thus simulate large length scales obliquely to the streamwise direction.

The incompressible Navier-Stokes equations are simulated using a spectral-element ( $x'$ - $y$ ) - Fourier ( $z'$ ) code [25]. The boundary conditions are no-slip at the moving plates and periodic in the  $x'$  and  $z'$  directions. The spatial resolution for the  $L_{x'} \times L_y \times L_{z'} = 10 \times 2 \times 120$  domain is  $N_x \times N_y \times N_z = 61 \times 31 \times 1024$ , consistent with that previously used at these values of  $Re$  [5, 8, 9]. Results have also been verified at higher resolutions.

We make two comments distinguishing our approach. Experimentalists [13, 14, 15] varied  $Re$  and reported the properties of the resulting patterns: in particular they measured angles and wavelengths varying from  $\theta = 25^\circ$  and  $\lambda_{z'} = 46$  at  $Re = 394$  to  $\theta = 37^\circ$  and  $\lambda_{z'} = 60$  at  $Re = 340$ . (They extrapolated the domain of existence to be  $325 \leq Re \leq 415$ .) In contrast, we fix the pattern angle and wavelength: in this way, we can determine the boundaries in parameter space within which each pattern can exist. Second, all the turbulent states we report are bistable with simple Couette flow. A major goal [6, 7, 10, 11], not addressed here, has been the determination

of lifetimes and transition probabilities of turbulent flow as a function of amplitude and  $Re$ .

We begin with simulations exploring the dependence of patterns on  $Re$ . To allow the system sufficient freedom to select different states, we set  $L_{z'} = 120$ , two to three times the experimentally observed wavelength. We fix  $\theta = 24^\circ$ , near its observed value at pattern onset. Figures 3(a) and (b) show two long series of simulations spanning the range  $290 \leq Re \leq 500$ . Space-time diagrams are shown for decreasing and increasing  $Re$  in discrete steps over time. In each case, kinetic energy fluctuations are on the right and principle peaks in associated spatial Fourier transforms are on the left.

More specifically, we compute  $E = |\mathbf{u} - \mathbf{u}_C|^2/2$  at 32 points equally spaced in  $z'$  along a line ( $x' = y = 0$ ) in the mid-channel. We compute  $E_{\text{rms}}$ , the rms of  $E$  in time windows of size  $T = 250$ . This gives a measure of the flow's turbulent intensity on a space-time grid. (Other measures such as the rms of individual velocity components gives similar results.) Time windows in Fig. 3(a) show  $E$  from which  $E_{\text{rms}}$  is computed at two points on the space-time grid. For the spectra on the left, we compute the instantaneous spatial Fourier transform  $\hat{E}_m$  of  $E$  for the same 32 points in the mid-channel. We take the modulus (to remove phase information) and average over windows of length  $T = 500$  to obtain  $\langle |\hat{E}_m| \rangle$ .

In Fig. 3(a) a turbulent flow is initialized at  $Re = 500$  by perturbing simple Couette flow. We call the resulting unpatterned state *uniform turbulence*. Its spectrum is flat.  $Re$  is decreased quickly to 350 where a pattern forms with three distinct turbulent and laminar regions. The  $m = 3$  spectral peak emerges. The selected wavelength of 40 agrees closely with experiment [13, 14, 15].  $Re$  is kept at 350 long enough to show that this pattern is stable. The final flow at  $Re = 350$  is visualized in Fig. 1. The pattern remains qualitatively the same through  $Re = 320$ .  $E_{\text{rms}}$  is systematically greater to the left of the band center. (Note that, due to the imposed tilt, there is no reflection symmetry in  $z'$ .) At  $Re = 310$  the pattern loses one turbulent region, accompanied by the emergence of the  $m = 2$  spectral peak. At  $Re = 300$ , a single turbulent region remains, and finally, at  $Re = 290$ , the flow reverts to simple Couette flow.

Figure 3(b) shows states obtained by increasing  $Re$  starting from  $Re = 350$ . The steady three-banded pattern persists up through  $Re = 390$ . At  $Re = 400$  and 410 the pattern is no longer steady: bands are less well defined and laminar regions appear and disappear (see below). Uniform turbulence is obtained at  $Re = 420$ .

We now present evidence that the patterns in Fig. 3 represent three qualitatively different states. The banded state at  $Re = 350$  is fundamentally *spatially periodic*. To support this we show in Fig. 4 a simulation at  $Re = 350$  in a domain whose length  $L_{z'}$  is slowly increased. The pattern adjusts to keep the wavelength in the approximate range 35–65 by splitting the turbulent bands when they

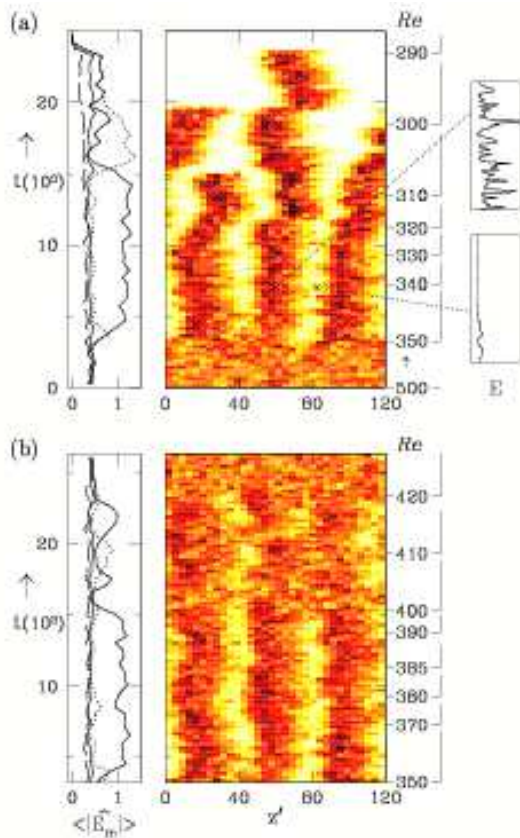


FIG. 3: Space-time evolution of turbulent-laminar patterns in the domain  $L_{x'} \times L_{z'} = 10 \times 120$ ,  $\theta = 24^\circ$ . Time evolves upward with changes in  $Re$  indicated on the right. Grayscale or color plots: kinetic energy fluctuations  $E_{rms}$  on a space-time grid. The same scale is used for all space-time plots, with  $E_{rms} = 0$  in white. Insets: kinetic energy plotted over a time window  $T = 250$  in a turbulent and laminar region. Left: Spectral peaks in the averaged spatial Fourier transform of kinetic energy with  $m = 3$  (solid) and  $m = 2$  (dotted), 0 (long-dashed), and 1 (short-dashed). (a) States seen upon decreasing  $Re$ , from uniform turbulence at  $Re = 500$ , through various patterned states, ending in simple Couette flow at  $Re = 290$ . (b) States seen upon increasing  $Re$ , from the three-banded laminar-turbulent pattern at  $Re = 350$  to uniform turbulence at  $Re = 420$ .

grow too large. The instantaneous integrated energy profile  $\bar{E} \equiv \int dx' dy E(x', y, z', t)$  is plotted at the final time. Between the turbulent bands,  $E$  does not reach zero and the flow, while basically laminar, differs from the simple Couette solution  $y\mathbf{e}_x$ .

In sharp contrast, the single turbulent patch seen in Fig. 3(a) prior to return to laminar Couette flow is a *localized state*. Figure 4 shows that in a domain of increasing size at  $Re = 300$  a single turbulent region of approximately fixed extent persists, independent of  $L_{z'}$ . Moreover,  $\bar{E}$  decays to zero exponentially as the flow approaches the simple Couette solution away from the patch. The localized states in our computations neces-

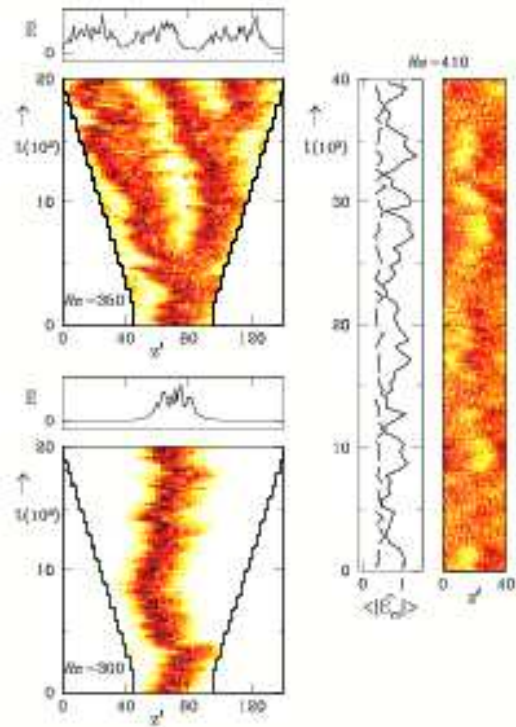


FIG. 4: Simulations at  $Re = 350$ ,  $Re = 300$ , and  $Re = 410$  illustrating three distinct states: periodic, localized, intermittent. Space-time representation of  $E_{rms}$  is as in Fig. 3. For  $Re = 350$  and  $Re = 300$  the domain length is increased from  $L_{z'} = 50$  to  $L_{z'} = 140$  in increments of 5. The integrated energy profile  $\bar{E}(z')$  is shown at the final time. For  $Re = 410$  a single long simulation is shown for  $L_{z'} = 40$ , accompanied by  $m = 1$  (solid) and  $m = 0$  (dashed) spectral peaks.

sarily take the form of bands when visualized in the  $x-z$  plane [e.g., Fig. 5(d) below]. Isolated bands and spots are reported experimentally [13, 14, 15] near these values of  $Re$ .

The third behavior is displayed by the *intermittent state* in Fig. 3 near the transition to uniform turbulence. Figure 4 shows a long simulation at  $Re = 410$  in a domain  $L_{z'} = 40$ . The flow never stabilizes but instead quasi-laminar regions nucleate and disappear continually. The range of  $E_{rms}$  in the space-time plot is noticeably smaller than for the stable patterns. Simulations with  $L_{z'} = 60$  show similar behavior. These states have been interpreted in [13, 14, 15] as resulting from noise-driven competition between banded patterns at equal and opposite angles. However, the intermittency is captured in our simulations, even though the competition between states of opposite angles is absent.

We have increased and decreased  $Re$  gradually at  $L_{z'} = 40$  and  $L_{z'} = 60$  and find no hysteresis in any of the transitions between the turbulent states.

We have explored regions of existence for various states as a function of  $Re$ , wavelength, and tilt. By varying  $L_{z'}$

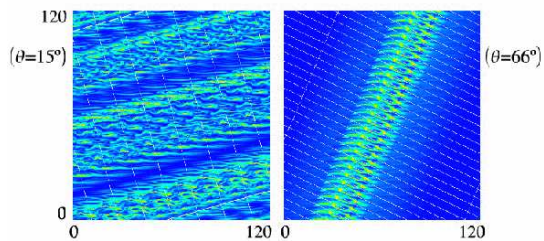


FIG. 5: Turbulent-laminar patterns at minimum ( $\theta = 15^\circ$ ) and maximum ( $\theta = 66^\circ$ ) angle for which they have been computed at  $Re = 350$ . Conventions as in Fig. 1.

at  $\theta = 24^\circ$ ,  $Re = 350$ , we have determined that the minimum wavelength is 35 and the maximum is 65. For  $L_{z'} \lesssim 30$ , uniform turbulence is obtained. For  $L_{z'} \gtrsim 70$  two bands of wavelength  $L_{z'}/2$  form (as in Fig. 4). This range of allowed wavelengths is nearly independent of  $Re$  wherever we have been able to compute banded states. Figure 5 shows a banded state at  $\theta = 15^\circ$  and a localized state at  $\theta = 66^\circ$ , the minimum and maximum angles for which we have thus far obtained patterns for  $L_{z'} = 120$ ,  $Re = 350$ . These extreme states may not be stable without the imposed periodicity of the computations. The sequence of states seen for increasing  $\theta$  at  $Re = 350$  is qualitatively the same as that for decreasing  $Re$  at  $\theta = 24^\circ$ . At  $\theta = 0^\circ$  and  $\theta = 90^\circ$  we do not find patterns, but only either uniform turbulence or simple Couette flow, with transition boundaries  $Re \approx 300$  for  $\theta = 0^\circ$  and  $Re \approx 390$  for  $\theta = 90^\circ$ . Full details will be reported elsewhere.

In past years minimal-flow-unit simulations have been used to great effect in understanding shear turbulence. We have shown that the same philosophy can be employed in the study of large-scale structures formed in turbulent flows. Specifically, we have reported the first simulations of turbulent-laminar patterns in plane Couette flow by numerically solving the Navier-Stokes equations in domains with a single long direction. The other dimensions are just large enough to resolve the inter-plate distance and to contain an integer number of longitudinal vortex pairs or streaks. Thus we have demonstrated that the patterns are quasi one-dimensional and we have identified what we believe to be near-minimal conditions necessary for their formation. Key is that the computational domain be tilted obliquely to the streamwise direction of the flow, otherwise no patterns are observed. We have found periodic, localized, and intermittent states where similar states are observed experimentally. We have explored the patterns' dependence on Reynolds number and on imposed wavelength and tilt. The existence of localized states in our simulations is particularly interesting because this suggests that the basic physics of isolated turbulent spots can be captured without simulat-

ing two large lateral directions. Future studies of these states may shed light on the mechanisms responsible for laminar-turbulent patterns and for turbulent transition.

We thank Olivier Dauchot for valuable discussions and Ron Henderson for the use of `Prism`. We thank the CNRS and the Royal Society for supporting this work. The two CPU decades of computer time used for this research were provided by the IDRIS-CNRS supercomputing center under project 1119, and by the University of Warwick Centre for Scientific Computing (with support from JREI grant JR00WASTEQ).

---

\* barkley@maths.warwick.ac.uk;

[www.maths.warwick.ac.uk/~barkley](http://www.maths.warwick.ac.uk/~barkley)

† laurette@limsi.fr; [www.limsi.fr/Individu/laurette](http://www.limsi.fr/Individu/laurette)

- [1] J. Jiménez and P. Moin, *J. Fluid Mech.* **225**, 213 (1991).
- [2] A. Lundbladh and A. V. Johansson, *J. Fluid Mech.* **229**, 499 (1991).
- [3] F. Daviaud, J. Hegseth, and P. Berge, *Phys. Rev. Lett.* **69**, 2511 (1992).
- [4] N. Tillmark and P. H. Alfredsson, *J. Fluid Mech.* **235**, 89 (1992).
- [5] J. M. Hamilton, J. Kim, and F. Waleffe, *J. Fluid Mech.* **287**, 317 (1995).
- [6] O. Dauchot and F. Daviaud, *Phys. Fluids* **7**, 335 (1995).
- [7] A. Schmiegel and B. Eckhardt, *Phys. Rev. Lett.* **79**, 5250 (1997).
- [8] J. Schumacher and B. Eckhardt, *Phys. Rev. E* **63**, 046307 (2001).
- [9] F. Waleffe, *Phys. Fluids* **15**, 1517 (2003).
- [10] B. Hof, A. Juel, and T. Mullin, *Phys. Rev. Lett.* **91**, 244502 (2003).
- [11] H. Faisst and B. Eckhardt, *J. Fluid Mech.* (in press).
- [12] P. Manneville, *Theor. Comput. Fluid Dyn.* (in press).
- [13] A. Prigent, Ph.D. thesis, University Paris-Sud (2001).
- [14] A. Prigent, G. Gregoire, H. Chate, O. Dauchot, and W. van Saarloos, *Phys. Rev. Lett.* **89**, 014501 (2002).
- [15] A. Prigent, G. Gregoire, H. Chate, and O. Dauchot, *Physica D* **174**, 100 (2003).
- [16] D. Coles, *J. Fluid Mech.* **21**, 385 (1965).
- [17] R. P. Feynman, *Lecture Notes in Physics* (Addison-Wesley, Reading, 1964).
- [18] C. W. van Atta, *J. Fluid Mech.* **25**, 495 (1966).
- [19] C. D. Andereck, S. S. Liu, and H. L. Swinney, *J. Fluid Mech.* **164**, 155 (1986).
- [20] J. J. Hegseth, C. D. Andereck, F. Hayot, and Y. Pomeau, *Phys. Rev. Lett.* **62**, 257 (1989).
- [21] A. Goharzadeh and I. Mutabazi, *Eur. Phys. J. B* **19**, 157 (2001).
- [22] A. Cros and P. Le Gal, *Phys. Fluids* **14**, 3755 (2002).
- [23] S. Bottin, O. Dauchot, F. Daviaud, and P. Manneville, *Phys. Fluids* **10**, 2597 (1998).
- [24] D. Barkley and L. S. Tuckerman, *Phys. Fluids* **11**, 1187 (1999).
- [25] R. D. Henderson and G. E. Karniadakis, *J. Comput. Phys.* **122**, 191 (1995).